# Third harmonic scattering in liquids

David P. Shelton[a)]
*Department of Physics and Astronomy, University of Nevada, Las Vegas, Nevada 89154-4002, USA*

(Received 8 August 2018; accepted 13 November 2018; published online 11 December 2018)

Third harmonic scattering (THS) from liquids has been observed and analyzed in several recent papers. It is considered to be analogous to second harmonic scattering (hyper-Rayleigh scattering) and to provide a means for measuring the second hyperpolarizability tensor of molecules in a liquid. However, the observed signal for a pure solvent is in fact mainly due to coherent third harmonic generation followed by Rayleigh scattering and direct incoherent THS (direct THS) makes only a small contribution (<2% for parallel polarized THS). This invalidates the internal reference method and the polarization analysis that has been applied for pure liquids. Theoretical comparison for the two processes, extensive experimental measurements for $CCl_4$ liquid, $SiO_2$ glass, and $CCl_2F_2$ gas and survey measurements for $D_2O$, $CDCl_3$, $CD_3CN$, and $(CD_3)_2SO$ liquid, are presented. *Published by AIP Publishing.* https://doi.org/10.1063/1.5051450

## I. INTRODUCTION

Third harmonic scattering (THS) is the nonlinear optical process where a laser beam at frequency $\omega$ produces scattered light at frequency $3\omega$. THS has only recently been explored as an experimental technique to measure the molecular second hyperpolarizability tensor $\gamma_{\alpha\beta\gamma\delta}(-3\omega;\omega,\omega,\omega)$.[1–4] It is considered to be analogous to the lower-order incoherent second harmonic scattering (SHS) process, also called hyper-Rayleigh scattering (HRS), which is widely used to measure the molecular first hyperpolarizability tensor $\beta_{\alpha\beta\gamma}(-2\omega;\omega,\omega)$.[5–8] The advantages of incoherent scattering measurements over coherent wave mixing and harmonic generation techniques are potential access to more hyperpolarizability tensor components by polarization analysis and great experimental simplicity.

THS has been used to measure molecular hyperpolarizability in pure liquids and chromophore solutions.[1–3] Relative hyperpolarizability determinations are simple when the intensity of incoherent harmonic scattering from each component of a solution is linear in molecular number density and quadratic in molecular hyperpolarizability. However, absolute calibration of the hyperpolarizability from THS measurements is problematic. In contrast, accurate gas-phase second hyperpolarizabilities are available for many atoms and molecules.[9] A possible way to produce an accurate absolute calibration for the hyperpolarizability of the molecules in a liquid THS reference sample is by comparison with THS for a gas sample.[10] When this was attempted, it became clear that THS from the sample was not incoherent THS, but was instead coherent third harmonic generation (THG) followed by Rayleigh scattering (RS). This has important implications for the interpretation of THS measurements. In the following, first, the theory will be outlined and then the results of THS measurements for $CCl_4$ liquid, $SiO_2$ glass, and $CCl_2F_2$ gas will be presented.

## II. THEORY

Consider THS produced by a focused, linear polarized, single mode, fundamental Gaussian laser beam with a confocal parameter $z_0$ in a medium with refractive index $n_1$. The beam is described by[11–13]

$$E_1(r,z,t) = E_0(1+i\xi)^{-1}\exp\left[\frac{-k_1 r^2}{2z_0(1+i\xi)}\right]\exp i(k_1 z-\omega_1 t), \tag{1}$$

where $E_0$ is the electric field amplitude at the center of the beam waist ($r = z = 0$), $\xi = z/z_0$, $k_1 = n_1\omega_1/c = 2\pi n_1/\lambda_0$, and $\lambda_0$ is the vacuum wavelength for light with frequency $\omega_1$. The radius $w_0$ of the beam at the waist ($1/e^2$ intensity) is given by the relation $\lambda_0 z_0 = n_1\pi w_0^2$, and the incident beam power is given by the integral of the intensity $\frac{1}{2}n_1\varepsilon_0 c|E_1(r,z,t)|^2$ over the beam cross section

$$P_1(z) = \tfrac{1}{4}\varepsilon_0 c\lambda_0 z_0|E_0|^2. \tag{2}$$

The molecular dipole oscillating at $\omega_3 = 3\omega_1$ induced by the electric field $E_1$ of the incident beam is[14,15]

$$\mu_3 = \tfrac{1}{24}L_1^3 L_3\gamma E_1^3, \tag{3}$$

where $L_1 = (n_1^2+2)/3$ and $L_3 = (n_3^2+2)/3$ are the Lorentz local field factors at $\omega_1$ and $\omega_3 = 3\omega_1$ for the medium, and for simplicity, just the rank 0 (scalar) irreducible part of the tensor $\gamma$ is included. The third harmonic scattered power at $\theta_s = 90°$ scattering angle, from one molecule, is[16]

$$\left(\frac{dP_3}{d\Omega}\right)_{\mathrm{THS}} = \tfrac{1}{2}n_3\varepsilon_0 c\left(\frac{\omega_3}{c}\right)^4\left|\frac{\mu_3}{4\pi\varepsilon_0}\right|^2, \tag{4}$$

a)shelton@physics.unlv.edu

and the THS power obtained from the incoherent sum over molecules with number density $\rho$ is

$$\left(\frac{dP_3(r,z)}{d\Omega dV}\right)_{\rm THS} = \frac{1}{2}n_3\varepsilon_0 c\rho\left(\frac{\omega_3}{c}\right)^4(4\pi\varepsilon_0)^{-2}(\tfrac{1}{24}L_1^3L_3\gamma E_0^3)^2 \times(1+\xi^2)^{-3}\exp\left[\frac{-3k_1r^2}{z_0(1+\xi^2)}\right]. \quad (5)$$

Integrating over the beam cross section gives

$$\left(\frac{dP_3(z)}{d\Omega dz}\right)_{\rm THS} = \frac{1}{2}n_3\varepsilon_0 c\rho\left(\frac{\omega_3}{c}\right)^4(4\pi\varepsilon_0)^{-2}(\tfrac{1}{24}L_1^3L_3\gamma E_0^3)^2 \times(1+\xi^2)^{-2}\frac{\pi z_0}{3k_1}, \quad (6)$$

and integrating once more over $z$ gives the total scattered power

$$\left(\frac{dP_3}{d\Omega}\right)_{\rm THS} = \frac{1}{2}n_3\varepsilon_0 c\rho\left(\frac{\omega_3}{c}\right)^4(4\pi\varepsilon_0)^{-2}(\tfrac{1}{24}L_1^3L_3\gamma E_0^3)^2\frac{\pi^2z_0^2}{6k_1}. \quad (7)$$

Finally, expressing the total THS power in terms of the incident beam power $P_1 = \frac{1}{4}\varepsilon_0 c\lambda_0 z_0|E_0|^2$ gives

$$\left(\frac{dP_3}{d\Omega}\right)_{\rm THS} = \frac{\rho}{6\pi\varepsilon_0^4c^2\lambda_0^2}\left(\frac{\omega_3}{c}\right)^4(\tfrac{1}{24}L_1^3L_3)^2\langle\gamma^2\rangle\frac{n_3}{n_1z_0}P_1^3. \quad (8)$$

Contributions from irreducible parts of the $\gamma$ tensor of all rank are included in the isotropic average of the squared $\gamma$ tensor, $\langle\gamma^2\rangle$, appearing in the final expression.[4] The analogous calculation for second harmonic scattering (HRS) mediated by the first hyperpolarizability tensor $\beta$ gives

$$\left(\frac{dP_2}{d\Omega}\right)_{\rm HRS} = \frac{\rho}{16\pi\varepsilon_0^3c\lambda_0}\left(\frac{\omega_2}{c}\right)^4(\tfrac{1}{4}L_1^2L_2)^2\langle\beta^2\rangle\frac{n_2}{n_1}P_1^2 \quad (9)$$

which differs from the THS result in that it has no $z_0$ dependence. (The $z_0^2$ factor exactly cancels when the HRS expression analogous to Eq. (7) is re-expressed in terms of incident power using $P_1 = \frac{1}{4}\varepsilon_0 c\lambda_0 z_0|E_0|^2$.)

Third harmonic generation (THG) is coherent forward scattering produced by the nonlinear polarization $P_{\rm NL} = \rho\mu_3$, and the propagating coherent third harmonic wave is the solution of[13]

$$(\nabla^2 - \mu\varepsilon\frac{\partial^2}{\partial t^2})E_3 = \mu\frac{\partial^2}{\partial t^2}P_{\rm NL}. \quad (10)$$

The paraxial solution of Eq. (10) in the undepleted pump approximation is[11–13]

$$E_3(r,z,t) = \rho\frac{iz_0}{2n_3\varepsilon_0}\frac{\omega_3}{c}(\tfrac{1}{24}L_1^3L_3\gamma E_0^3)(1+i\xi)^{-1} \times\exp\left[\frac{-k_3r^2}{2z_0(1+i\xi)}\right]\exp i(k_3z-\omega t) \times\int_{-\infty}^{\xi}d\xi'\frac{\exp(i\Delta k_{13}z_0\xi')}{(1+i\xi')^2}, \quad (11)$$

where $\Delta k_{13} = (3k_1 - k_3) = 6\pi(n_1 - n_3)/\lambda_0$. The third harmonic beam power is given by the integral of the intensity $\frac{1}{2}n_3\varepsilon_0 c|E_3(r,z,t)|^2$ over the beam cross section

$$P_3(z) = \frac{1}{2}n_3\varepsilon_0 c\rho^2\left(\frac{z_0}{2n_3\varepsilon_0}\frac{\omega_3}{c}\right)^2(\tfrac{1}{24}L_1^3L_3\gamma E_0^3)^2 \times\frac{\pi z_0}{k_3}|I(\Delta k_{13}z_0,\xi)|^2, \quad (12)$$

where

$$I(\Delta k_{13}z_0,\xi) = \int_{-\infty}^{\xi}d\xi'\frac{\exp(i\Delta k_{13}z_0\xi')}{(1+i\xi')^2}. \quad (13)$$

The magnitude of the integral is in the range $0 \le |I(\Delta k_{13}z_0,\xi)| \le 1$ for transparent media with normal dispersion where $\Delta k_{13} \le 0$. The magnitude of the integral is maximum for $\xi = 0$ and is zero for $\xi = \pm\infty$. The magnitude of the integral at $\xi = 0$, $|I(\Delta k_{13}z_0, 0)|$, is an increasing function of $\Delta k_{13}z_0$ with limiting values $|I(-\infty, 0)| = 0$ and $|I(0, 0)| = 1$. Thus, a laser beam focused in an infinite medium produces a third harmonic beam with maximum power at the beam waist, $z = 0$, and with vanishing power at $z = \pm\infty$.

The integral in Eq. (12) for the THG beam power has $z$ dependence given by

$$|I(\Delta k_{13}z_0,\xi)|^2 = |I(\Delta k_{13}z_0,0)|^2(1+\xi^2)^{-c}, \quad (14)$$

where the exponent $c(\Delta k_{13}z_0)$ is a decreasing function of $\Delta k_{13}z_0$, with limiting values $c(-\infty) = 2$ and $c(0) = 1$. The $z$ integral of Eq. (12) for the THG beam power gives

$$\int_{-\infty}^{\infty}dzP_3(z) = \frac{1}{2}n_3\varepsilon_0 c\rho^2\left(\frac{z_0}{2n_3\varepsilon_0}\frac{\omega_3}{c}\right)^2(\tfrac{1}{24}L_1^3L_3\gamma E_0^3)^2 \times\frac{\pi^2{z_0}^2}{2k_3}|I(\Delta k_{13}z_0,0)|^2\,F(\Delta k_{13}z_0), \quad (15)$$

where

$$F(\Delta k_{13}z_0) = \left(\frac{2}{\pi}\right)\int_{-\infty}^{\infty}d\xi\left|\frac{I(\Delta k_{13}z_0,\xi)}{I(\Delta k_{13}z_0,0)}\right|^2 \quad (16)$$

is an increasing function of $\Delta k_{13}z_0$, with limiting values $F(-\infty) = 1$ and $F(0) = 2$. Figure 1 shows the graphs of the functions $|I(\Delta k_{13}z_0, 0)|$, $c(\Delta k_{13}z_0)$, and $F(\Delta k_{13}z_0)$.

Rayleigh scattering of the third harmonic beam localized near the waist of the incident laser beam produces indirect THS, labelled as THG*RS. The scattered power is

$$\left(\frac{d^2P_3(z)}{d\Omega dz}\right)_{\rm THG^*RS} = P_3(z)R_{90}(\omega_3), \quad (17)$$

where $P_3(z)$ is the THG beam power and $R_{90}$ is the Rayleigh scattering ratio at $\theta_s = 90°$ for linear polarized incident light. Rayleigh scattering is proportional to the mean square thermodynamic fluctuation of the dielectric constant $\varepsilon$, and the Rayleigh ratio $R_{90}$ is given by[17–19,]

$$R_{90}(\omega) = \frac{k_BT\beta_T}{16\pi^2}\left(\frac{\omega}{c}\right)^4\left[\rho\left(\frac{\partial\varepsilon}{\partial\rho}\right)_T\right]^2 = \frac{k_BT\beta_T}{16\pi^2}\left(\frac{\omega}{c}\right)^4(n^2-1)^2\left(\frac{n^2+2}{3}\right)^2, \quad (18)$$

where $\beta_T$ is the isothermal compressibility. Applying the Clausius-Mosotti relation[16,17]

$$\rho\alpha/3\varepsilon_0 = (\varepsilon-1)/(\varepsilon+2) = (n^2-1)/(n^2+2) \quad (19)$$

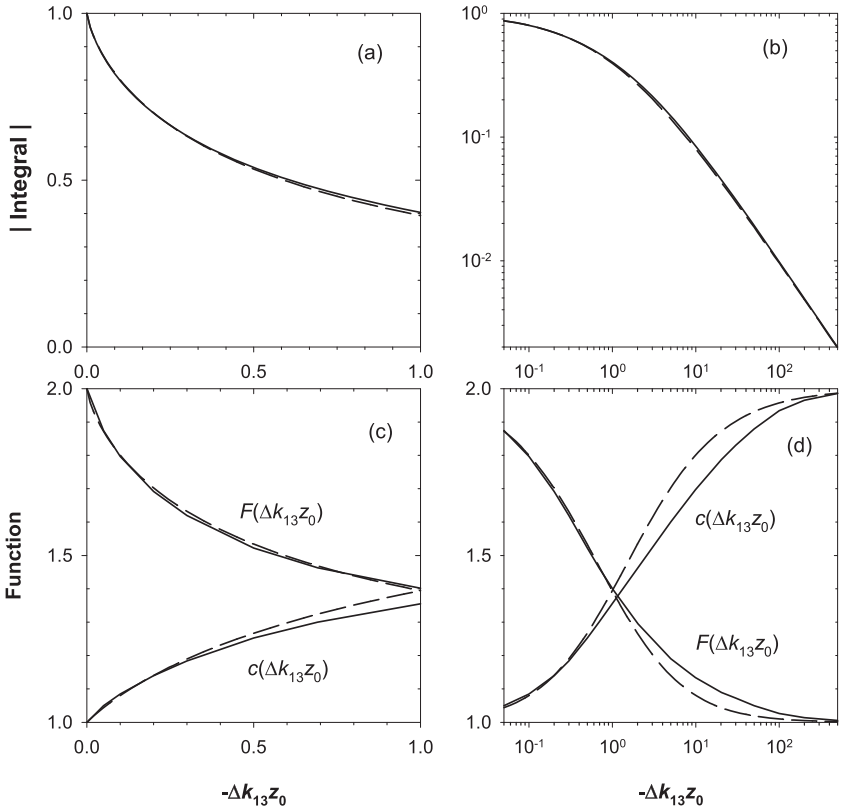


FIG. 1. Graphs of the integral $|I(\Delta k_{13}z_0, 0)|$ for small values (a) and a wider range of values (b) of $|\Delta k_{13}z_0|$, and graphs of the functions $c(\Delta k_{13}z_0)$ and $F(\Delta k_{13}z_0)$ for small values (c) and a wider range of values (d) of $|\Delta k_{13}z_0|$. The integral $|I(\Delta k_{13}z_0, 0)|$ gives the THG amplitude at the beam waist, $c(\Delta k_{13}z_0)$ is the exponent in the stretched Lorentzian function describing the variation of the THG intensity away from the beam waist, and $F(\Delta k_{13}z_0)$ is the integral of the normalized THG intensity over the beam path. The dashed curves in (a) and (b) show the function $f(x) = (1 + x^a)^{-1/a}$ approximating the integral, where $x = -\Delta k_{13}z_0$ and $a = 0.745$. The dashed curves in (c) and (d) show the functions $g(x) = 1 + (1 + x^a)^{-1/a}$ approximating $F(\Delta k_{13}z_0)$ and $h(x) = 1 + x\,(1 + x^a)^{-1/a}$ approximating $c(\Delta k_{13}z_0)$. The maximum error is 5% for the approximate functions.

for the molecular polarizability $\alpha$, this becomes

$$R_{90}(\omega) = k_B T \beta_T L^4 \left(\frac{\omega}{c}\right)^4 \left(\frac{\rho\alpha}{4\pi\varepsilon_0}\right)^2. \tag{20}$$

For a gas described by the virial equation of state,[20] with second and third virial coefficients $B$ and $C$, the compressibility is

$$k_B T \beta_T = -\frac{k_B T}{V}\left(\frac{\partial V}{\partial p}\right)_T = \rho^{-1}(1 + 2B\rho + 3C\rho^2)^{-1} \tag{21}$$

and the Rayleigh ratio is

$$R_{90}(\omega) = \rho L^4 \left(\frac{\omega}{c}\right)^4 \left(\frac{\alpha}{4\pi\varepsilon_0}\right)^2 (1 + 2B\rho + 3C\rho^2)^{-1}. \tag{22}$$

The total THG*RS scattered power obtained by integrating Eq. (17) over $z$ is

$$\left(\frac{dP_3}{d\Omega}\right)_{\text{THG*RS}} = \frac{1}{2} n_3 \varepsilon_0 c \rho^2 \left(\frac{z_0}{2n_3\varepsilon_0}\frac{\omega_3}{c}\right)^2 \left(\frac{1}{24} L_1^3 L_3 \gamma E_0^3\right)^2 \times \frac{\pi^2 z_0^2}{2k_3} |I(\Delta k_{13}z_0, 0)|^2 F(\Delta k_{13}z_0) R_{90}(\omega_3). \tag{23}$$

Finally, expressing the total THG*RS power in terms of the incident beam power $P_1 = \frac{1}{4}\varepsilon_0 c \lambda_0 z_0 |E_0|^2$ gives

$$\left(\frac{dP_3}{d\Omega}\right)_{\text{THG*RS}} = \frac{\rho^2}{54\pi\varepsilon_0^4 c^2}\left(\frac{\omega_3}{c}\right)^4 \left(\tfrac{1}{24} L_1^3 L_3\right)^2 \langle\gamma\rangle^2 \frac{z_0}{n_3^2} P_1^3 \times |I(\Delta k_{13}z_0, 0)|^2 F(\Delta k_{13}z_0) R_{90}(\omega_3), \tag{24}$$

where $\langle\gamma\rangle^2$, the squared isotropic average of $\gamma$, appears instead of $\langle\gamma^2\rangle$ that appears in Eq. (8) for THS.

The expression for THG*RS from a gas that is obtained by combining Eqs. (22) and (24) has $\rho^3$ density dependence, as compared to linear density dependence in Eq. (8) for direct THS. The scattered light intensity variation along the beam path is the same for THG*RS and direct THS for materials with large dispersion such that $|\Delta k_{13}z_0| >> 1$ and $c = 2$, but for $|\Delta k_{13}z_0| << 1$ and $c = 1$, the THG*RS source cylinder is elongated compared to the THS source. The ratio of Eqs. (24) and (8) gives a simple expression for the relative total scattered power for THG*RS and direct THS. The ratio is

$$\frac{P_{\text{THG*RS}}}{P_{\text{THS}}} = \left(\frac{\pi^2 n_1^3}{9n_3^3}\right)\frac{\langle\gamma\rangle^2}{\langle\gamma^2\rangle}\rho w_0^4 |I(\Delta k_{13}z_0, 0)|^2 \times F(\Delta k_{13}z_0) R_{90}(\omega_3), \tag{25}$$

where $\lambda_0 z_0 = n_1 \pi w_0^2$ relating the confocal parameter $z_0$ and the beam waist radius $w_0$ has been used. Low molecular number density and tight focusing (small $\rho w_0^4$) increases the relative contribution of direct THS compared to THG*RS.

Table I presents the results of evaluating Eq. (25) with $\langle\gamma^2\rangle = \langle\gamma\rangle^2$ for three representative materials and typical experimental conditions. The refractive indices for $CCl_4$ and $SiO_2$ are experimentally measured values.[12,21] The Rayleigh ratio for $CCl_4$ is obtained using Eq. (18) with experimentally measured $n_3$ and $\beta_T$,[17] and is consistent with direct measurements.[22,23] The Rayleigh ratio for $SiO_2$ is from experimentally measured scattering[24–26] and compressibility.[27] The refractive index for $CCl_2F_2$ gas is determined from the experimental

TABLE I. Material parameters and relative intensity for THG*RS and direct THS predicted by Eq. (25) with $\langle\gamma^2\rangle = \langle\gamma\rangle^2$ for a laser beam at $\lambda_0 = 1064$ nm focused to $w_0 = 4.5\,\mu$m in three materials, $CCl_4$ liquid, $SiO_2$ glass, and $CCl_2F_2$ gas ($\rho = \rho_{\mathrm{STP,i}}$, where $\rho_{\mathrm{STP,i}}$ is the density of an ideal gas at 0 °C and 1 atm), all at $T = 25$ °C. References are given in superscript.

| | $CCl_4$ liquid | $SiO_2$ glass | $CCl_2F_2$ gas |
|---|---|---|---|
| $\rho$ ($m^{-3}$) | $6.20 \times 10^{27}$ | $2.20 \times 10^{28}$ | $2.68 \times 10^{25}$ |
| $n_1$ | 1.446 78[21] | 1.449 67[21] | 1.001 127[28,29] |
| $n_3$ | 1.483 35[21] | 1.476 42[21] | 1.001 189[28,29] |
| $-\Delta n_{13}$ | 0.036 57 | 0.026 75 | $6.1 \times 10^{-5}$ |
| $z_0$ ($\mu$m) | 87 | 87 | 60 |
| $-\Delta k_{13} z_0$ | 56.4 | 41.2 | 0.065 |
| $c(\Delta k_{13} z_0)$ | 1.89 | 1.86 | 1.06 |
| $F(\Delta k_{13} z_0)$ | 1.047 | 1.060 | 1.851 |
| $\lvert I(\Delta k_{13} z_0, 0)\rvert$ | 0.017 2 | 0.023 2 | 0.846 1 |
| $R_{90}$ ($m^{-1}$ $sr^{-1}$) | $7.58 \times 10^{-3}$ [17] | $7.8 \times 10^{-4}$ [24,25] | $1.37 \times 10^{-4}$ |
| $P_{\mathrm{THG^*RS}}/P_{\mathrm{THS}}$ | 6.04 | 4.17 | 2.19 |

values $\alpha = 7.52 \pm 0.02 \times 10^{-40}$ $C^2$ $m^2$ $J^{-1}$ at $\lambda_0 = 633$ nm from Ref. 28 and $-\Delta k_{12} = 9.8 \pm 0.1$ $cm^{-1}$ for $\lambda_0 = 694.3$ nm and $\rho = \rho_{\mathrm{STP,i}}$ from Ref. 29, using Eq. (19) and assuming a dispersion relation with the form $n(\nu) - 1 = \rho(a + b\nu^2)$. The Rayleigh ratio for $CCl_2F_2$ gas at $\rho = \rho_{\mathrm{STP,i}} = 44.615$ mol $m^{-3}$ is calculated using Eq. (22), with virial coefficients $B = -480$ $cm^3$ $mol^{-1}$ and $C = 20\,000$ $cm^6$ $mol^{-2}$,[20] and is consistent with direct measurements.[30] Table I shows that THG*RS is several times larger than direct THS in all three materials.

In the usual THS experiment, the laser beam is focused into a rectangular cell containing the sample and the light scattered near 90° scattering angle is collected from length $D$ of the focal cylinder over a fixed external solid angle. Compared to the case where the sample cell is empty, the effect of refraction at the windows of the filled sample cell is to increase the laser beam confocal parameter by the factor of $n_1$ (the beam waist radius $w_0$ at the focus is unchanged) and to decrease the collection solid angle inside the sample by a factor $n_3^2$. The actual observed scattering is given by

$$\left(\frac{dP_3}{d\Omega'}\right)_{\mathrm{obs}} = n_3^{-2} f(c, n_1 z_{0,0}, D)\left(\frac{dP_3}{d\Omega}\right), \tag{26}$$

where $z_{0,0}$ ($z_0 = n_1 z_{0,0}$) is the confocal parameter in the empty (filled) cell and the field of view factor is

$$f(c, n_1 z_{0,0}, D) = \frac{\int_{-D/2}^{D/2} [1 + (z/n_1 z_{0,0})^2]^{-c} dz}{\int_{-\infty}^{\infty} [1 + (z/n_1 z_{0,0})^2]^{-c} dz}. \tag{27}$$

Reflections at the cell windows reduce the laser power in the sample and the collected light signal, and are accounted for by the product of window transmission factors $T_1^3 T_3$ for light at $\omega_1$ and $\omega_3$, where $T = 1 - (n_s - n_w)^2/(n_s + n_w)^2$ for the sample-window interface. These effects may be important when comparing different samples under otherwise identical conditions. The calculations above considered a single transverse and longitudinal mode laser beam, and the results are slightly modified for a multi-longitudinal mode laser beam. In the case where there are many modes with the random phase, the average third harmonic power is increased by a factor of $\langle P_1^3\rangle/\langle P_1\rangle^3 = 6$ due to the chaotic intensity fluctuations of the laser beam.[31]

The calculations above were done assuming that all electric field vectors are parallel to each other and perpendicular to the horizontal scattering plane. The signal measured in this configuration is denoted $S_{\mathrm{VV}}$, where the first (second) subscript denotes the incident (scattered) field polarization. Other polarization configurations important for the analysis of the present experiments are $S_{\mathrm{HV}}$ and $S_{\mathrm{CV}}$, with horizontal and circular polarized incident laser beams, respectively. The isotropic tensor $\langle\gamma\rangle$ mediating THG has non-vanishing components $\langle\gamma\rangle_{\alpha\alpha\alpha\alpha} = \langle\gamma\rangle_{\alpha\alpha\beta\beta} + \langle\gamma\rangle_{\alpha\beta\alpha\beta} + \langle\gamma\rangle_{\alpha\beta\beta\alpha}$ and produces THG which is polarized parallel to incident linear polarization and vanishes for incident circular polarization.[14,32] However, depolarized THG*RS ($S_{\mathrm{HV}}$) can result due to depolarized RS of the polarized THG beam. The THG*RS signal $S_{\mathrm{EV}}$ for an elliptical polarized incident field $E_0(\cos\psi\,\hat{e}_{\mathrm{V}} + i\sin\psi\,\hat{e}_{\mathrm{H}})$ and 90° scattering angle is given by

$$S_{\mathrm{EV}} \propto (\cos^2\psi + \rho_{\mathrm{V}}\sin^2\psi)(\cos^2\psi - \sin^2\psi)^2, \tag{28}$$

where $\rho_{\mathrm{V}}$ is the depolarization ratio for Rayleigh scattering of linear polarized light, and $S_{\mathrm{VV}}$, $S_{\mathrm{CV}}$, and $S_{\mathrm{HV}}$ are obtained for $\psi = 0°$, 45°, and 90°, respectively.

For direct THS, the isotropic average of the squared $\gamma$ tensor $\langle\gamma^2\rangle$ has contributions from the irreducible parts of $\gamma$ with ranks 0, 1, 2, 3, and 4, producing polarized and depolarized THS, and non-zero THS for circular polarized incident light.[2,4] In the most general case, the following relation holds for direct THS at 90° scattering angle:[4]

$$2S_{\mathrm{CV}} = (S_{\mathrm{VV}} + S_{\mathrm{HV}}). \tag{29}$$

For $T_d$ symmetry molecules, where the non-vanishing irreducible parts of $\gamma$ are $\gamma^{(0)}$ and $\gamma^{(4)}$ with ranks 0 and 4, one has $1/2 \le S_{\mathrm{CV}}/S_{\mathrm{VV}} \le 13/16$, with the minimum (maximum) attained when $\gamma^{(4)}$ ($\gamma^{(0)}$) vanishes.[4] The variation of $S_{\mathrm{EV}}(\psi)/S_{\mathrm{VV}}$ with $\psi$ in the most general case is qualitatively similar for direct THS [Eq. (4) in Ref. 2] and THG*RS [Eq. (28)]. The most prominent difference is that $S_{\mathrm{EV}}(\psi)/S_{\mathrm{VV}}$ at $\psi = 45°$ is $\ge 1/2$ for direct THS but vanishes for THG*RS.

## III. EXPERIMENT

Harmonic scattering was measured using the apparatus previously employed for HRS measurements.[33] The beam from a multi-longitudinal-mode Nd:YAG (yttrium aluminium garnet) laser (operating at $\lambda_0 = 1064$ nm, 4.3 kHz repetition rate, 100 ns pulse duration, and 0.5 $cm^{-1}$ spectral width) is focused to a $w_0 = 4.5$ $\mu$m beam waist radius in the sample. The polarization of the laser beam is set by a linear polarizer and liquid crystal variable wave plate (LCVWP), and 90° scattered light is collected and collimated by an aspheric lens (focal length $f = 4$ mm, maximum numerical aperture $NA = 0.5$), analyzed by a linear polarizer, focused into an optical fiber, and fiber-coupled to a spectral filter followed by the photon counting detector. The sample temperature was $T = 25.0$ °C, and the laser beam average power in the sample was up to $P_{\mathrm{av}} = 3.6$ W.

Harmonic scattering was measured for three materials: $CCl_4$ liquid, $SiO_2$ glass, and $CCl_2F_2$ gas, with the material parameters given in Table I. The $CCl_4$ sample was contained in a standard 10 mm square cuvette. The $SiO_2$ sample was a 2 mm × 10 mm cuvette with the beam propagating inside the 5 mm thick fused silica glass wall. The $CCl_2F_2$ sample was contained in a 2 mm × 10 mm cuvette (at pressure up to 6 atm.) with the beam propagating perpendicular to the 5 mm thick walls, along a 2 mm beam path in the gas. The $CCl_4$ ($CCl_2F_2$) sample cell was filled through a 0.2 $\mu$m (0.5 $\mu$m) particle filter. Adjustments were made to precisely position the harmonic scattering source at the focal point of the collection lens (1 mm inside the sample), at the center of the field of view defined by the optical fiber. The field of view with a 600 $\mu$m fiber and 2.7× magnification is about 220 $\mu$m in diameter, slightly larger than the 170 $\mu$m length ($2z_0$) of the scattering source cylinder in $CCl_4$. Third harmonic light at $\lambda = 355$ nm was selected (and second harmonic light at 532 nm was blocked) by a tandem pair of 355 nm UV bandpass filters with 10 nm and 1 nm bandwidth. Second harmonic measurements could also be made by switching to a 532 nm bandpass filter with 2 nm bandwidth. The α-BBO (barium borate) analyzing prism polarizer, lenses, and fiber were selected for high UV transmission.

The third harmonic signal is nearly cubic in the average laser power $P_{av}$ for all three samples, as shown in Fig. 2(a). Self-focusing[34,35] in $CCl_4$ ($SiO_2$) caused the beam waist to move towards the focusing lens by 5.5 $\mu$m/W (3.8 $\mu$m/W), so position adjustments were made to maintain the beam waist on the collection optic axis during scattered light measurements. Figures 2(b) and 2(c) show that $S_{VV}/P_{av}^3$ still had a small power dependence, +0.5%/W ± 0.3%/W for $CCl_4$ and −1.2%/W ± 0.7%/W for $SiO_2$. The self-focusing threshold measured at 796 nm and scaled to 1064 nm (using $\lambda^2$ scaling)[34] is 4.5 MW for $CCl_4$ and 7.7 MW for $SiO_2$.[35] The estimated $S_{VV}/P_{av}^3$ variation with $P_{av}$, based on laser peak power and the self-focusing threshold power, is +0.3%/W for $CCl_4$, consistent with the observed variation. For $SiO_2$, the estimated variation due to self-focusing is +0.2%/W, and the observed variation is larger and has the opposite sign, indicating a contribution from three-photon absorption for $SiO_2$. Self-focusing is not observed for the $CCl_2F_2$ gas sample, and $S_{VV}/P_{av}^3$ in Fig. 2(d) shows no significant variation. Table II gives the values for $S_{VV}/P_{av}^3$ measured at $P = 3.6$ W and extrapolated to $P = 0$, for $CCl_4$ liquid, $SiO_2$ glass, and $CCl_2F_2$ gas (at $\rho = 5.94\rho_{STP,i}$).

Figure 3 shows HRS measurements for $CCl_2F_2$ gas as a function of gas density. The gas density was determined from $p$ and $T = 25$ °C using the virial equation of state with coefficients $B = -480$ cm$^3$ mol$^{-1}$ and $C = 20\,000$ cm$^6$ mol$^{-2}$.[20] The density virial correction is 15% at the highest pressure. The HRS signal is nearly linear in density, and the deviation from linearity is accounted for by the factor $L_1^4L_2^2T_1^2T_2n_1^{-1.4}n_2^{-1}$, as shown in Fig. 3(b). This factor is obtained by combining Eqs. (9) and (26) and using the approximate result $f \approx n_1^{-0.4}$ obtained from Eq. (27) for $c = 1$, $z_{0,0} = 60$ $\mu$m, and $D = 220$ $\mu$m by expressing Eq. (27) as a power series in $(n_1 - 1)$ for $(n_1 - 1) << 1$.

Figure 4 shows THS measurements for $CCl_2F_2$ gas as a function of gas density. The THS signal is nearly cubic in density, consistent with THG*RS rather than direct THS which has linear density dependence. Figure 4(b) shows the deviation from cubic density dependence, which is fit by the function obtained by combining Eqs. (22) and (24)–(26)

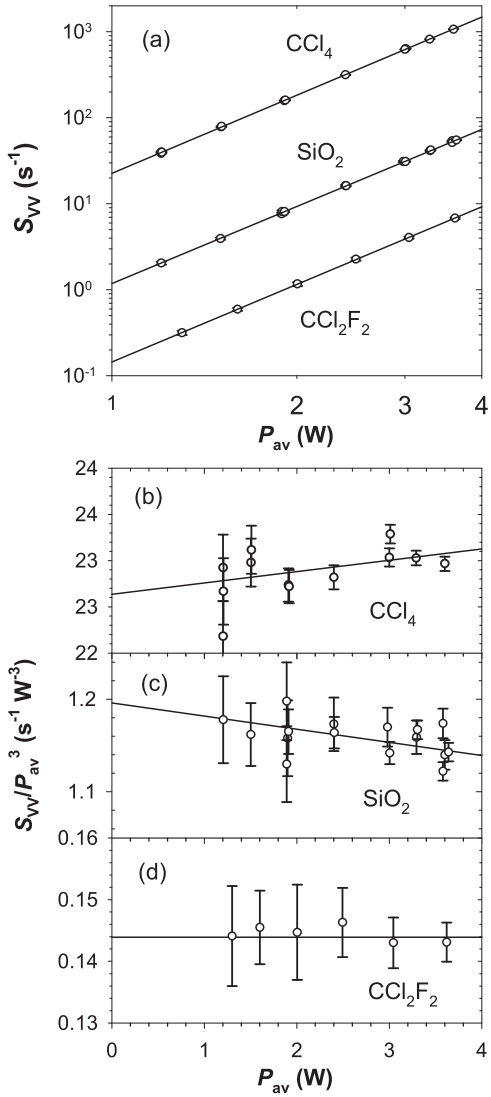


FIG. 2. Third harmonic signal $S_{VV}$ versus average laser power $P_{av}$. (a) Log-log graph of $S(P)$ for three materials. The small deviations from $S \propto P^3$ are shown by the graphs of $S/P^3$ versus $P$ for (b) $CCl_4$, (c) $SiO_2$, and (d) $CCl_2F_2$ ($\rho = 5.94\rho_{STP,i}$).

$$r^{-3}S/P^3 = a_3L_1^6L_3^6T_1^3T_3n_1^{0.6}n_3^{-4}(1 + 2B\rho + 3C\rho^2)^{-1} \times r^{-2}[(rG_{THG}^{1/2} + W_{THG})^2 + G_{THS}], \quad (30)$$

TABLE II. Third harmonic signals $S_3 = (S_{VV}/P_{av}^3)_{P=0}$ measured at $P_{av} = 3.6$ W and extrapolated to $P = 0$. The $CCl_2F_2$ measurement is for gas density $\rho = 5.94\rho_{STP,i}$. The ratios for $\chi^{(3)}$ and $\gamma$ are calculated from $S_3$ using Eqs. (35)–(37).

| | $CCl_4$ | $SiO_2$ | $CCl_2F_2$ |
|---|---|---|---|
| $S_3$ (s$^{-1}$ W$^{-3}$) | 33.4 ± 0.3 | 1.70 ± 0.02 | 0.144 ± 0.003 |
| $\chi^{(3)}/\chi^{(3)}_{CCl4}$ | 1 | 0.511 ± 0.003 | 2.75 ± 0.03×10$^{-3}$ |
| $\gamma/\gamma_{CCl4}$ | 1 | 0.144 ± 0.001 | 0.375 ± 0.004 |

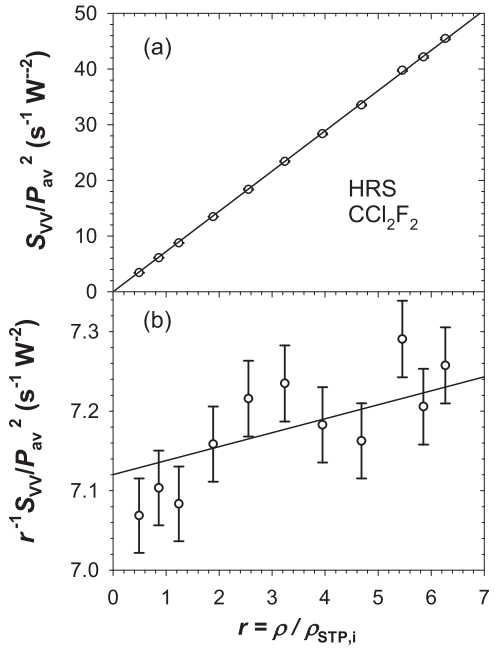


FIG. 3. Second harmonic signal $S_{VV}$ versus density $r = \rho/\rho_{STP,i}$ for $CCl_2F_2$ gas. (a) The graph shows the data (circles) fit by $S/P^2 \propto r$ (line). (b) Deviations from $S/P^2 \propto r$ are shown by the graph of $r^{-1}S/P^2$ versus $r$. The curve shows the theoretical function $r^{-1}S/P^2 = a_2 L_1^4 L_2^2 T_1^2 T_2 n_1^{-1.4} n_2^{-1}$ with the adjustable parameter $a_2$ fit to the data (circles, with 0.66% error bars due to 0.26% laser power fluctuations and 0.4% photon counting statistics).

where the gas THG factor

$$G_{THG} = \frac{|I(\Delta k_{13} z_0, 0)|^2 F(\Delta k_{13} z_0)}{[|I(\Delta k_{13} z_0, 0)|^2 F(\Delta k_{13} z_0)]_{r=1}} \tag{31}$$

is normalized at gas density $r = 1$, and the adjustable parameters are $a_3$ and $W_{THG}$. The parameter $W_{THG}$ represents the amplitude of the THG wave from the entrance window, and $G_{THS}$ represents the direct THS contribution from the gas. The value $G_{THS} = 0.622$ is determined by the value $P_{THG^*RS}/P_{THS} = 2.19$ at $r = 1$ with $W_{THG} = 0$ from Table I, taking into account that Eq. (27) for the field of view factor at the experimental conditions is 1.36 times larger for THS as compared to RS*THG. The value $W_{THG} = -1.04$ for the fit indicates that the window THG nearly cancels the gas THG at $r = 1$. The sign and magnitude of $W_{THG}$ from the fit agree with the sign and magnitude of THG estimated using Eq. (12) for the $SiO_2$ window of the gas cell. The window THG and gas THS contributions estimated from this fit are significant even at the highest gas density, reducing the signal by a factor of 1.76 for the measurement at $r = 5.94$ in Table II. The window THG contribution to the signal could be reduced by using a longer gas cell.

Figure 5 shows the measurements of the polarization dependence of the third harmonic signal for $CCl_4$ and $SiO_2$, from which the relative contributions of THG*RS and direct THS can be determined. Table III gives the values (extrapolated to zero collection solid angle, $NA = 0$) for the polarization ratios $S_{HV}/S_{VV}$ and $S_{CV}/S_{VV}$. The observed THS polarization ratios $S_{HV}/S_{VV}$ match the corresponding depolarization ratios $\rho_V$ for Rayleigh scattering of polarized light by $CCl_4$ and $SiO_2$.[22,25,26] This indicates that the signals are due to THG*RS, although a direct THS contribution is not excluded.

The signal $S_{CV}$ is entirely due to direct THS since THG for a circular polarized beam is zero.[14,32] The THG*RS contribution due to imperfect circular polarization for this measurement is $S_{CV}/S_{VV} \leq 10^{-5}$, since quarter wave retardation for the LCVWP is set within about 1 mrad and $S_{CV}$ is quadratic in angle and retardation errors. Equation (29) combined with the observed ratio $S_{CV}/S_{VV}$ gives the upper bound

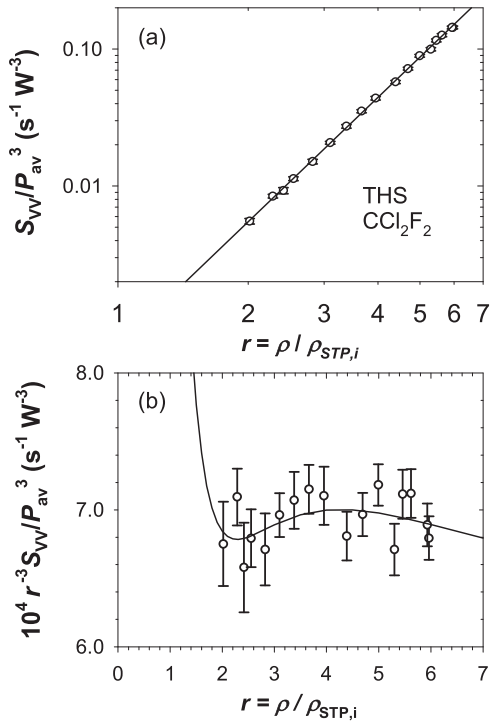


FIG. 4. Third harmonic signal $S_{VV}$ versus density $r = \rho/\rho_{STP,i}$ for $CCl_2F_2$ gas. (a) Log-log graph shows data (circles) fit by $S/P^3 \propto r^3$ (line). (b) Deviations from $S/P^3 \propto r^3$ are shown by the graph of $r^{-3}S/P^3$ versus $r$. The curve shows the theoretical function given by Eq. (30) fit to the data (circles).

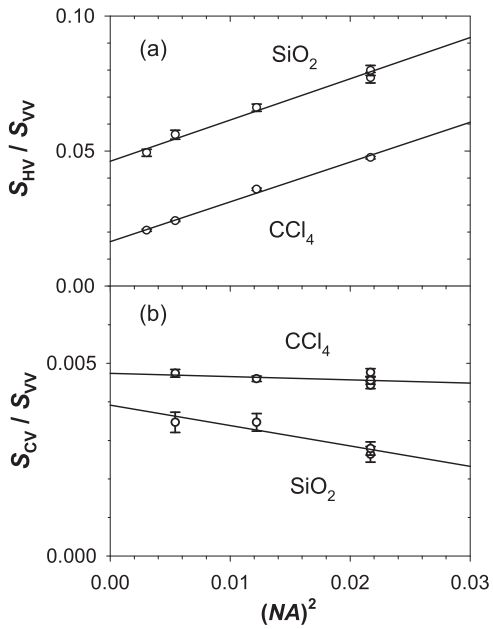


FIG. 5. Third harmonic signal ratios for polarizations (a) $S_{HV}/S_{VV}$ and (b) $S_{CV}/S_{VV}$, extrapolated to zero collection solid angle ($NA = 0$).

TABLE III. THS polarization ratios $S_{HV}/S_{VV}$ and $S_{CV}/S_{VV}$ at $NA = 0$ from Fig. 5 are shown. $S_{HV}/S_{VV}$ is comparable to $\rho_V$, the RS depolarization ratio for polarized light. The lower bound $S_{VV,THG^*RS}/S_{VV,THS}$ for the ratio of THG*RS and direct THS contributions is determined from $S_{CV}/S_{VV}$ using Eq. (32). The lower bound for the THS reduction factor $S_{THS,i}/S_{THS}$ from Eq. (33) is comparable to the RS reduction factor given by the compressibility ratio $\beta_{T,i}/\beta_T$. References are given in superscript.

| | $CCl_4$ | $SiO_2$ |
|---|---|---|
| $S_{HV}/S_{VV}$ | 0.017 ± 0.001 | 0.046 ± 0.002 |
| $S_{CV}/S_{VV}$ | 0.0047 ± 0.0002 | 0.0039 ± 0.0003 |
| $\rho_V$ | 0.021[22] | 0.044 ± 0.002[25,26] |
| $S_{VV,THG^*RS}/S_{VV,THS}$ | 106 ± 5 | 128 ± 10 |
| $S_{THS,i}/S_{THS}$ | 18 | 31 |
| $\beta_{T,i}/\beta_T$ | 37[17] | 39[25,27] |

$$S_{VV,THS}/S_{VV} \le 2S_{CV}/S_{VV} \tag{32}$$

for the direct THS contribution to the total signal. An upper bound <1% for the direct THS contribution is obtained from the $S_{CV}/S_{VV}$ results for $SiO_2$ and $CCl_4$ in Table III. Table IV summarizes the $S_{CV}/S_{VV}$ results for $SiO_2$ and $CCl_4$, and also the measurements at $NA = 0.15$ for four additional liquids. The largest direct THS contribution to $S_{VV}$ is <2%.

From the upper bound for $S_{VV,THS}/S_{VV}$ given by Eq. (32), one obtains a lower bound for $S_{VV,THG^*RS}/S_{VV,THS}$, shown for $SiO_2$ and $CCl_4$ in Table III. The values for $S_{VV,THG^*RS}/S_{VV,THS}$ in Table III are larger than the corresponding values for $P_{THG^*RS}/P_{THS}$ given in Table I, by the factor

$$S_{THS,i}/S_{THS} = \frac{S_{VV,THG^*RS}/S_{VV,THS}}{P_{THG^*RS}/P_{THS}} \tag{33}$$

also shown in Table III. This is the factor by which the incoherent sum over molecules, assumed in the derivation of Eq. (8), overestimates $P_{THS}$. The overestimate occurs because thermodynamic density fluctuations are much smaller for a liquid or glass than for an ideal gas with the same density. This is the same effect as occurs for RS, where Eq. (22) evaluated for an ideal gas overestimates RS from a liquid or glass by the factor $\beta_{T,i}/\beta_T$, with $\beta_{T,i} = (\rho k_B T)^{-1}$ and $\beta_T$ the measured compressibility.[17,25,27] The lower bound $S_{THS,i}/S_{THS}$ for the THS overestimate is consistent with $\beta_{T,i}/\beta_T$ shown in Table III. In contrast, this effect does not reduce HRS since it is governed by molecular orientation fluctuations not density fluctuations. (Dipolar HRS vanishes for a centrosymmetric medium, but orientation fluctuations can break local centrosymmetry and effectively randomize the scattered phase to produce HRS, whereas density fluctuations do not.) From the results above, the actual total THS intensity is larger than the intensity calculated assuming completely incoherent direct THS, by the lower bound factor

$$S/S_{THS,i} = [(\beta_{T,i}/\beta_T)(2S_{CV}/S_{VV})]^{-1}. \tag{34}$$

From Eq. (34) and the data in Table III, one calculates $S/S_{THS,i} = 2.9$ for $CCl_4$ and 3.3 for $SiO_2$.

The third harmonic signal measurements $S_3 = (S_{VV}/P_{av}^3)_{P=0}$ given in Table II can be used to estimate nonlinear susceptibilities $\chi^{(3)} = \rho L_1^3 L_3 \gamma$ and hyperpolarizabilities $\gamma$. From Eqs. (24) and (26), one sees that $\chi^{(3)} \propto (S_3/F_3)^{1/2}$ where

$$F_3 = T_1^3 T_3 n_1 n_3^{-4} f(c, z_0, D)|I(\Delta k_{13} z_0, 0)|^2 F(\Delta k_{13} z_0) R_{90}(\omega_3). \tag{35}$$

Table II gives the values calculated for

$$\chi^{(3)}/\chi^{(3)}_{CCl4} = (S_3/F_3)^{1/2}/(S_3/F_3)^{1/2}_{CCl4}, \tag{36}$$

$$\gamma/\gamma_{CCl4} = (\chi^{(3)}/\rho L_1^3 L_3)/(\chi^{(3)}/\rho L_1^3 L_3)_{CCl4}. \tag{37}$$

The result $\chi^{(3)}_{SiO2}/\chi^{(3)}_{CCl4} = 0.511 \pm 0.003$ in Table II is in rough agreement with $\chi^{(3)}_{SiO2}/\chi^{(3)}_{CCl4} = 0.39 \pm 0.02$ from previous THG measurements at $\lambda = 1064$ nm.[12] The result $\gamma_{CCl2F2}/\gamma_{CCl4} = 0.375 \pm 0.004$ in Table II is in rough agreement with $\gamma_{CCl2F2}/\gamma_{CCl4} = 0.445 \pm 0.010$ from previous gas phase ESHG (electric field induced second harmonic generation) measurements at $\lambda = 694.3$ nm.[29] A second value $\gamma_{CCl2F2}/\gamma_{CCl4} = 0.375 \times (1.76)^{1/2} = 0.497 \pm 0.005$ is obtained by accounting for the estimated window THG and gas direct THS contributions to the measured THS signal. The previous ESHG result falls between these two estimates. The stated error bars represent the statistical uncertainty of the measurements and do not include the systematic uncertainty of the $CCl_2F_2$ gas THS measurement mainly due to window THG. The systematic uncertainty due to window THG could be eliminated by using a longer gas cell with an absorbing entrance window.

TABLE IV. THS polarization ratio $S_{CV}/S_{VV}$ for silica glass and five liquids, at $NA = 0$ for $SiO_2$ and $CCl_4$ and at $NA = 0.15$ for the others. The upper bounds on the direct THS contributions given by $S_{VV,THS}/S_{VV} \le 2S_{CV}/S_{VV}$ are all <2%.

| Material | $S_{CV}/S_{VV}$ |
|---|---|
| $SiO_2$ | 0.0039 ± 0.0003 |
| $D_2O$ | 0.0042 ± 0.0004 |
| $CCl_4$ | 0.0047 ± 0.0002 |
| $CDCl_3$ | 0.0057 ± 0.0004 |
| $CD_3CN$ | 0.0067 ± 0.0006 |
| $(CD_3)_2SO$ | 0.0098 ± 0.0008 |

## IV. DISCUSSION AND CONCLUSION

The main result of this work is that THS from a pure liquid is produced by THG*RS with a negligible contribution from direct THS. THG in the forward direction has been used to measure $\chi^{(3)}$ and $\gamma$ of molecular liquids,[12,36,37] and measurements using THG*RS and THG are similar in many respects. One advantage of THG*RS over THG is that it does not vanish for a laser beam focused in an infinite medium, so a window does not need to be placed close to the focus, and the THG contribution from the windows can be made to effectively vanish for a long enough sample. This is the case for the 10 mm long $CCl_4$ liquid and $SiO_2$ glass samples in the present work, but not for a 2 mm long $CCl_2F_2$ gas sample. A disadvantage of THG*RS for accurate nonlinear optical property measurements is the need to also determine $R_{90}$ and the sensitivity of RS and THG*RS to the presence of particles.[38–40]

THS has recently been investigated as an alternative method for measuring the second hyperpolarizability $\gamma$ of

chromophore molecules in solution, analogous to the use of HRS for measuring the molecular first hyperpolarizability $\beta$, with the same advantages of simplicity and wide applicability.[1,2] The solvent was used as an internal calibration standard for determination of $\gamma$ from THS measurements, and THS polarization measurements were used to determine $\gamma$ tensor spherical invariant contributions. These studies assumed that direct THS was being observed, which is not correct for the solvent but may be correct for the dissolved chromophore.

The experimental conditions in the most recent THS studies are similar to the present experiment, with the beam focused to a waist diameter of 8 $\mu$m,[1,2,41] so THG*RS is expected to dominate the THS signal measured from $CCl_4$ and other pure solvents in those experiments. THS from chromophore solutions was also measured. For binary solutions with solvent A and chromophore B, the THG*RS signal is $\propto(\rho_A\gamma_A + \rho_B\gamma_B)^2$ (assuming that refractive index dispersion of the solution is not changed by the dissolved chromophore), while the direct THS signal is $\propto(\rho_A\gamma_A^2 + \rho_B\gamma_B^2)$. In Ref. 2, solutions of DR1 (disperse red 1) at concentrations up to $\rho_B = 0.1$ mM in $CH_3CN$ ($\rho_A = 19.1$M) were measured, where $\gamma_B/\gamma_A \approx 2000$. In this experiment, a strong chromophore in dilute solution produces THS which is the sum of direct THS from the chromophore and THG*RS from the solvent. The total THS signal increases linearly with DR1 concentration, and at the maximum DR1 concentration, reaches a value that is $3 \times$ THG*RS from neat solvent. A calculation assuming completely incoherent direct THS for the solvent underestimates the reference intensity by about a factor of three [see Eq. (34)], so the internal reference method gives chromophore $\gamma_B$ about 1.7× too small. In Ref. 1, solutions of stilbene at concentrations up to $\rho_B = 0.6$M in $CHCl_3$ ($\rho_A = 12.5$M) were measured, where $\gamma_B/\gamma_A \approx 7$. For these solutions, both solvent and chromophore contribute significantly to THG, giving THG*RS $\propto (1 + 0.34y_B)^2$ where $0 < y_B < 1$ is the fraction of maximum stilbene concentration, and THG*RS increases almost linearly (with small upward curvature) over the measured stilbene concentration range. Direct THS is mainly from the chromophore, since $\rho_B\gamma_B^2/\rho_A\gamma_A^2 \approx 2$ and THS due to density fluctuations is more strongly suppressed for the dense solvent than for the more dilute chromophore. The observed concentration dependence in Fig. 3 of Ref. 1 is roughly linear and is fit by the sum of THG*RS and direct THS, with the maximum direct THS about 1.4× pure solvent THG*RS. Using THG*RS $\propto(1 + 0.34y_B)^2$ with the solvent as the internal reference gives $\gamma_B/\gamma_A = 7.1$, in accidentally close agreement with $\gamma_B/\gamma_A = 7.0$ obtained in Ref. 1 using the solvent as the internal reference and assuming only direct THS. In this experiment, a weak chromophore at high concentration produces THS which is the sum of direct THS and THG*RS from the chromophore and THG*RS from the solvent.

THS polarization dependence was measured in Ref. 2 for $CCl_4$, $CH_2Cl_2$, and for a solution of DR1 in $CH_3CN$. The results $S_{HV}/S_{VV} = 0.017$ for $CCl_4$ and 0.23 for $CH_2Cl_2$ are consistent with either direct THS or THG*RS for these liquids, but the result $S_{CV}/S_{VV} = 0.11$ measured for both liquids requires combined direct THS and THG*RS. The $S_{HV}/S_{VV}$ value measured for $CCl_4$ in Ref. 2 agrees with the result of the present work in Table III, whereas the $S_{CV}/S_{VV}$ value measured for $CCl_4$ disagrees. For the DR1 solution, the results are $S_{HV}/S_{VV} = 0.16$ and $S_{CV}/S_{VV} = 0.41$, consistent with contributions from both direct THS and THG*RS. Analysis of polarization data in terms of spherical invariants of $\gamma$ has been proposed[2,4] and can be applied to chromophore solution polarization data with the solvent contribution subtracted, but pure solvent polarization data contain almost no information about the $\gamma$ tensor components since the signal is almost entirely due to THG*RS.

In summary, THS from a strong chromophore in dilute solution may be due to incoherent direct THS analogous to HRS, but THS from the solvent is mainly Rayleigh scattered coherent THG (THG*RS). This invalidates the internal reference method, where the solute molecule hyperpolarizability is calibrated by comparison to the solvent molecules in the same sample, with all experimental factors other than the molecular number densities cancelling out in the comparison. THS is still a convenient way to measure the second hyperpolarizability $\gamma$ of chromophores in solution, and relative calibration can be achieved by comparison of sample and reference chromophores in dilute solutions with the same solvent, but absolute calibration remains problematic. The polarization analysis of THS that has been applied to pure liquids is invalid since the signal is THG*RS, but this analysis is valid when applied to direct THS from a strong chromophore in dilute solution.


[1] N. van Steerteghem, K. Clays, T. Verbiest, and S. van Cleuvenbergen, Anal. Chem. **89**, 2964 (2017).
[2] V. Rodriguez, J. Phys. Chem. C **121**, 8510 (2017).
[3] T. Yamada and S. Mashiko, Jpn. J. Appl. Phys., Part 2 **39**, L1060 (2000).
[4] J. S. Ford and D. L. Andrews, J. Phys. Chem. A **122**, 563 (2018).
[5] K. Clays and A. Persoons, Phys. Rev. Lett. **66**, 2980 (1991).
[6] P. Kaatz and D. P. Shelton, J. Chem. Phys. **105**, 3918 (1996).
[7] P. K. Das, J. Phys. Chem. B **110**, 7621 (2006).
[8] J. Campo, F. Desmet, W. Wenseleers, and E. Goovaerts, Opt. Express **17**, 4587 (2009).
[9] D. P. Shelton and J. E. Rice, Chem. Rev. **94**, 3 (1994).
[10] P. Kaatz, E. A. Donley, and D. P. Shelton, J. Chem. Phys. **108**, 849 (1998).
[11] J. F. Ward and G. H. C. New, Phys. Rev. **185**, 57 (1969).
[12] F. Kajzar and J. Messier, Phys. Rev. A **32**, 2352 (1985).
[13] A. Yariv, *Quantum Electronics*, 3rd ed. (Wiley, New York, 1989).
[14] P. N. Butcher and D. Cotter, *The Elements of Nonlinear Optics* (Cambridge University Press, Cambridge, 1990).
[15] H. Reis, J. Chem. Phys. **125**, 014506 (2006).
[16] J. D. Jackson, *Classical Electrodynamics*, 3rd ed. (Wiley, New York, 1999).
[17] A. K. Burnham, G. R. Alms, and W. H. Flygare, J. Chem. Phys. **62**, 3289 (1975).
[18] G. D. Patterson, J. Chem. Phys. **63**, 4032–4034 (1975).
[19] X. Zhang and L. Hu, Opt. Express **17**, 1671–1678 (2009).
[20] J. H. Dymond and E. B. Smith, *The Virial Coefficients of Pure Gases and Mixtures* (Clarendon, Oxford, 1980).
[21] I. Rau, F. Kajzar, J. Luc, B. Sahraoui, and G. Boudebs, J. Opt. Soc. Am. B **25**, 1738 (2008).
[22] E. R. Pike, W. R. M. Pomeroy, and J. M. Vaughan, J. Chem. Phys. **62**, 3188 (1975).
[23] E. Moreels, W. DeCeuninck, and R. Finsy, J. Chem. Phys. **86**, 618–623 (1987).
[24] S. Schroder, M. Kamprath, A. Duparre, and A. Tunnermann, Opt. Express **14**, 10537 (2006).
[25] X. Chen, L. Ju, R. Flaminio, H. Luck, C. Zhao, and D. Blair, Opt. Commun. **284**, 4732 (2011).
[26] K. Saito, H. Kakiuchida, and A. J. Ikushima, J. Non-Cryst. Solids **222**, 329 (1997).

[27]C. Levelut, A. Faivre, R. LeParc, B. Champagnon, J.-L. Hazemann, and J.-P. Simon, Phys. Rev. B **72**, 224201 (2005).
[28]K. Kerl and H. Varchmin, Int. J. Thermophys. **12**, 171 (1991).
[29]C. K. Miller and J. F. Ward, Phys. Rev. A **16**, 1179 (1977).
[30]B. A. Bodhaine, Appl. Opt. **18**, 121 (1979).
[31]R. Loudon, *The Quantum Theory of Light*, 2nd ed. (Clarendon, Oxford, 1983).
[32]D. L. Andrews, J. Phys. B: At. Mol. Phys. **13**, 4091 (1980).
[33]D. P. Shelton, Rev. Sci. Instrum. **82**, 113103 (2011).
[34]Y. R. Shen, *The Principles of Nonlinear Optics* (Wiley, New York, 1984).
[35]A. Brodeur and S. L. Chin, Phys. Rev. Lett. **80**, 4406 (1998).
[36]G. R. Meredith, B. Buchalter, and C. Hanzlik, J. Chem. Phys. **78**, 1533 (1983).
[37]G. R. Meredith, B. Buchalter, and C. Hanzlik, J. Chem. Phys. **78**, 1543 (1983).
[38]R. B. Miles, W. R. Lempert, and J. N. Forkey, Meas. Sci. Technol. **12**, R33 (2001).
[39]V. I. Shcheslavskiy, S. M. Saltiel, A. Faustov, G. I. Petrov, and V. V. Yakovlev, J. Opt. Soc. Am. B **22**, 2402 (2005).
[40]H.-W. Zang, H.-L. Li, Y. Su, Y. Fu, M.-Y. Hou, A. Baltuska, K. Yamanouchi, and H. Xu, Opt. Lett. **43**, 615 (2018).
[41]V. Rodriguez, J. Grondin, F. Adamietz, and Y. Danten, J. Phys. Chem. B **114**, 15057 (2010).